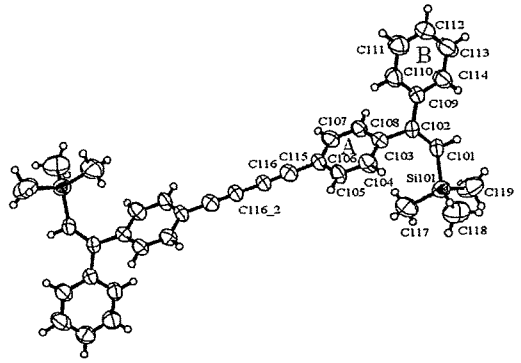

Fig. 2 Molecular structure of 1,4-bis(4-((Z)-1-phenyl-2-(trimethylsilyl)vinyl)phenyl)buta-1,3-diyne along with the atom and ring labelings. Thermal ellipsoids of non-H atoms are drawn at the 50% probability level.

Table 2 Selected bond lengths (Å), bond angles(°) and torsion angles(°)

molecule I		molecule II	
Si(101) - C(101)	1.869(4)	Si(201) - C(201)	1.857(3)
Si(101) - C(117)	1.858(5)	Si(201) - C(217)	1.843(5)
Si(101) - C(118)	1.847(5)	Si(201) - C(218)	1.858(5)
Si(101) - C(119)	1.854(4)	Si(201) - C(219)	1.862(4)
C(101) - C(102)	1.351(6)	C(201) - C(202)	1.347(5)
C(106) - C(115)	1.425(5)	C(206) - C(215)	1.450(5)
C(115) - C(116)	1.213(5)	C(215) - C(216)	1.182(5)
C(116) - C(116)[1]	1.372(5)	C(216) - C(216)[2]	1.394(4)
C(101) - Si(101) - C(117)	115.5(2)	C(201) - Si(201) - C(217)	115.8(2)
C(101) - Si(101) - C(118)	108.1(2)	C(201) - Si(201) - C(218)	108.3(2)
C(101) - Si(101) - C(119)	103.7(2)	C(201) - Si(201) - C(219)	104.3(2)
C(117) - Si(101) - C(118)	110.5(2)	C(217) - Si(201) - C(218)	111.5(2)
C(117) - Si(101) - C(119)	108.2(2)	C(217) - Si(201) - C(219)	107.8(2)
C(118) - Si(101) - C(119)	110.6(2)	C(218) - Si(201) - C(219)	108.8(2)
Si(101) - C(101) - C(102)	134.0(3)	Si(201) - C(201) - C(202)	135.4(2)
C(101)-C(102)-C(103)-C(104)	57.7(5)	C(201)-C(202)-C(203)-C(204)	57.6(5)
C(101)-C(102)-C(109)-C(110)	-152.9(4)	C(201)-C(202)-C(209)-C(210)	-151.8(4)
Si(101)-C(101)-C(102)-C(103)	8.6(6)	Si(201)-C(201)-C(202)-C(203)	9.3(5)
Si(101)-C(101)-C(102)-C(109)	-172.2(3)	Si(201)-C(201)-C(202)-C(209)	-172.2(2)
C(117)-Si(101)-C(101)-C(102)	11.6(5)	C(217)-Si(201)-C(201)-C(202)	12.2(4)
C(118)-Si(101)-C(101)-C(102)	-112.8(4)	C(218)-Si(201)-C(201)-C(202)	-113.8(4)
C(119)-Si(101)-C(101)-C(102)	129.8(4)	C(219)-Si(201)-C(201)-C(202)	130.4(4)

Symmetry operators: (1) $-x, -y+3, -z+1$ (2) $-x+2, -y+2, -z+2$.

are 100s and 200s are designated as molecules I and II, respectively. Selected bond lengths, bond angles and torsion angles are given in Table 2. The 1,4-diphenylbuta-1,3-diyne moiety takes a linear and planar structure. The molecules are centrosymmetric, and hence the trimethylsilyl and the terminal phenyl groups are located on opposite sides with respect to the central 1,3-diyne part. Two independent halves of the molecules take very similar structures. The hundreds of digits of atomic labels are omitted for the sake of simplicity in the following description. The geometrical parameters for molecule I are followed by the corresponding values for molecule II in square brackets. The dihedral angle between two phenyl planes is 106.2(2) [106.2(2)]°. The torsion angle of Si-C1-C2-C3 is 8.6(6) [9.3(5)]°. The trimethylsilyl group faces ring A. The C17 atom points to the center of ring A(Cg) with the C17···Cg distances being 3.71 [3.73]Å. Although the distances are not significantly short, this conformation indicates a weak attractive interaction between ring A and the methyl group. The bond angle of C17-Si-C1 is 115.5(2) [115.8(2)]°, which is significantly larger than the corresponding angles with respect to C18 and C19. The bond angle Si-C1-C2 is 134.0(3) [135.4(2)]°. The widening of these bond angles also suggests an interaction between C17 and ring A. The other bond angles and bond lengths in the molecules are within the expected ranges. The molecules are packed by van der Waals interactions in the crystal.

Acknowledgements

We thank the Research and Study Program of Tokai University Educational System General Research Organization for financial support.

References

1. J. N. Wilson, M. Josowicz, Y. Wang, and U. H. F. Bunz, *Chem. Commun.*, **2003**, 2962.
2. J. Tonggang, L. Yuliang, L. Huibiao, Y. Jianping, L. Xiaofeng, J. Li, Y. Mingjian, L. Junbo, L. Cuihong, W. Shu, and Z. Daoben, *Tetrahedron*, **2007**, *63*, 3168.

X-ray Structure Analysis Online 2009, VOL. 25

X-ray Structure Analysis Online

Crystal Structure of 1,4-Bis[4-((2Z)-(trimethylsilyl)-1-phenylethenyl)-phenylethynyl]benzene

Takumi KATAISHI,* Fumiaki ANZAI,* Taichi NAKANO,* Mieko HIRAYAMA, and Noriaki HIRAYAMA**†**

**Department of Materials Chemistry, School of High-Technology for Human Welfare, Tokai University, 317 Nishino, Numazu, Shizuoka 410-0395, Japan*

***Basic Medical Science and Molecular Medicine, Tokai University School of Medicine, 143 Shimokasuya, Isehara, Kanagawa 259-1143, Japan*

The crystal of the title compound, $Si_2C_{44}H_{42}$, belongs to space group $P2_1/c$ with cell dimensions of a = 11.8349(6), b = 8.5746(5), c = 18.6172(10)Å, β = 95.785(3)°. The final $R1$ [$I > 2\sigma(I)$] value is 0.0489. The central conjugated system composed of phenyleneethynylene groups takes a linear, but non-planar structure. The molecule has a center of symmetry. The dihedral angle between the central phenyl ring and the flanking phenyl ring is 18.7(1)°. The two trimethylsilyl groups are located on opposite sides of the molecule with respect to the central part.

(Received, April 9, 2009; Accepted May 29, 2009; Published on web October 10, 2009)

Organic compounds possessing a high degree of conjugation, such as poly(phenyleneethynylene)s, have been recognized as ideal materials for advanced electronic and photonic applications such as for organic LEDs, liquid-crystal displays and solar cells.[1] In aiming to obtain such functional materials, we have been undertaking a series of studies to synthesize a family of novel low-molecular-weight phenyleneethynylenes with terminal vinylsilane units. Although various phenyleneethynylenes have been synthesized, only a few phenyleneethynylenes with terminal vinylsilane unit(s) have been synthesized so far. Recently, we successfully synthesized the title compound (Fig. 1) by the Sonogashira-Hagihara cross-coupling of 1,4-diethynylbenzene with 2 equiv. of (Z)-1-(4-iodophenyl)-2-(trimethylsilyl)-1-phenylethene, being prepared by the Migita-Kosugi-Stille cross-coupling of 1,4-diiodobenzene with (Z)-1-(tributylstannyl)-2-(trimethylsilyl)-1-phenylethene,[2] in an isolated yield of 89%. An X-ray analysis was undertaken in order to disclose the inherent three-dimensional structure of this novel compound.

Single crystals were obtained from an ethyl acetate-hexane solution. A colorless platelet crystal with a size of 0.50 × 0.50 × 0.10 mm was mounted on a glass fiber and used for data collection. The structure was solved by direct methods, and non-H atoms were refined by a full-matrix least-squares method with anisotropic temperature factors. The positions of all H-atoms were located by a difference Fourier synthesis and refined by the riding model. In the final refinement, however, the atomic parameters of the H-atoms were fixed. The molecule has a center of symmetry. The crystal and experimental data are

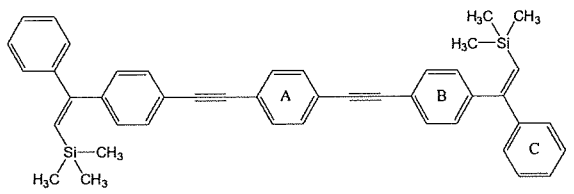

Fig. 1 Chemical structure of 1,4-bis[4-((2Z)-(trimethylsilyl)-1-phenylethenyl)phenylethynyl]benzene along with the ring labels.

Table 1 Crystal and experimental data

Chemical formula: $Si_2C_{44}H_{42}$	
Formula weight = 626.99	
T = 296 K	
Crystal system: monoclinic	Space group: $P2_1/c$
a = 11.8349(6)Å	
b = 8.5746(5)Å	β = 95.785(3)°
c = 18.617(1)Å	
V = 1633.6(2)Å^3	Z = 2
D_x = 1.108 g/cm^3	
Radiation: Cu K_α (λ = 1.54187 Å)	
μ(Cu K_α) = 1.056 mm^{-1}	F(0 0 0) = 668
Crystal size = 0.50 × 0.50 × 0.10 mm^3	
No. of reflections collected = 17010	
No. of independent reflections= 3339	
θ_{max} = 67.5° with Cu K_α	
Data/Restraints/Parameters = 3336/0/208	
Goodness-of-fit on F^2 = 0.885	
R indices [$I > 2\sigma(I)$]: $R1$ = 0.0489	
R indices (all data): $R1$ = 0.0549, $wR2$ = 0.1392	
$(\Delta/\sigma)_{max}$ = 0.000	
$(\Delta\rho)_{max}$ = 0.18 e/Å^3 $(\Delta\rho)_{min}$ = –0.40 e/Å^3	
Measurement: Rigaku RAXIS-RAPID	
Program system: CrystalStructure 3.7.0[3]	
Structure determination: SIR92[4]	
CCDC deposition number: 726795	

† To whom correspondence should be addressed.
E-mail: hirayama@is.icc.u-tokai.ac.jp

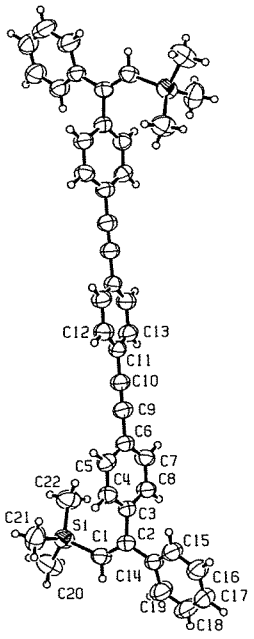

Fig. 2 Molecular structure of 1,4-bis[4-((2Z)-(trimethylsilyl)-1-phenylethenyl)phenylethynyl]benzene along with the atom labels. Thermal ellipsoids of non-H atoms are drawn at the 50% probability level.

given in Table 1.

A stereoscopic drawing of the molecule prepared by ORTEP-III[5] is shown in Fig. 2. Selected bond lengths, bond angles and torsion angles are given in Table 2. The central conjugated system composed of phenyleneethynylene groups take a linear, but non-planar structure. The two trimethylsilyl groups are located on opposite sides of the molecule with respect to the central conjugated part. The dihedral angle between the central phenyl ring A and the flanking phenyl ring B is 18.7(1)°, which indicates that the conjugated system takes an appreciably non-planar structure. The dihedral angle between the terminal phenyl ring C and the rings A and B are 72.4(1) and 90.9(1)°, respectively. The terminal phenyl ring is nearly perpendicular to the ring B. The C1-C2-C3-C4 torsion angle of 68.5(2)° indicates that the silyl group is also significantly deviated from the central conjugated system. The C1-Si-C22 bond angle is 113.86(9)°, and it is significantly larger than those of C1-Si-C20 and C1-Si-C21. The C22 atom points to the center of the ring

Table 2 Selected bond lengths (Å), bond angles (°) and torsion angles (°)

Si(1)-C(1)	1.864(2)	Si(1)-C(20)	1.862(2)
Si(1)-C(21)	1.867(2)	Si(1)-C(22)	1.866(2)
C(2)-C(3)	1.493(2)	C(6)-C(9)	1.437(2)
C(9)-C(10)	1.193(2)	C(10)-C(11)	1.433(2)
C(1)-Si(1)-C(20)	106.5(1)	C(1)-Si(1)-C(21)	109.0(1)
C(1)-Si(1)-C(22)	113.86(9)	C(20)-Si(1)-C(21)	108.9(1)
C(20)-Si(1)-C(22)	108.5(1)	C(21)-Si(1)-C(22)	109.9(1)
Si(1)-C(1)-C(2)	131.49(13)	C(1)-C(2)-C(3)	119.8(1)
C(1)-C(2)-C(14)	123.31(14)	C(3)-C(2)-C(14)	116.8(1)
C(2)-C(14)-C(15)	120.55(15)	C(2)-C(14)-C(19)	122.4(2)
C(6)-C(9)-C(10)	177.4(2)	C(9)-C(10)-C(11)	178.2(2)
C(20)-Si(1)-C(1)-C(2)	155.2(2)	C(21)-Si(1)-C(1)-C(2)	-87.4(2)
C(22)-Si(1)-C(1)-C(2)	35.7(2)	Si(1)-C(1)-C(2)-C(3)	-1.1(2)
Si(1)-C(1)-C(2)-C(14)	176.2(1)	C(5)-C(6)-C(9)-C(10)	-90(4)
C(7)-C(6)-C(9)-C(10)	89(4)	C(6)-C(9)-C(10)-C(11)	-69(9)
C(9)-C(10)-C(11)-C(12)	178(3)	C(9)-C(10)-C(11)-C(13)	-3(4)

B(Cg) with the C22···Cg distances being 3.54 Å. It indicates a weak attractive interaction between the ring B and this methyl group. The bond angle of C1-C2-C14 is significantly larger than that of C3-C2-C14, presumably due to a steric repulsion between hydrogen atoms attached to the C1 and C19 atoms with the H···H distance of 2.21 Å. The molecules are packed by van der Waals interactions in the crystal.

Acknowledgements

We thank the Research and Study Program of Tokai University Educational System General Research Organization for financial support.

References

1. T. Jiu, Y. Li, H. Liu, L. Jiang, M. Yuan, J. Li, C. Li, S. Wang, and D. Zhu, *Tetrahedron*, **2007**, *63*, 3168.
2. K. Sonogashira, K. Thoda, and N. Hagihara, *Tetrahedron Lett.*, **1975**, 4467.
3. CrystalStructure, verSion 3.5.1, **2000 – 2003**, Crystal Structure Analysis Package, Rigaku and Rigaku/MSC.
4. SIR92: A. Altomare, G. Cascarano, C. Giacovazzo, A. Guagliardi, M. Burla, G. Polidori, and M. Camalli, *J. Appl. Cryst.*, **1994**, *27*, 435.
5. ORTEP III, L. J. Farrugia, *J. Appl. Cryst.*, **1997**, *22*, 389.

Journal of Cerebral Blood Flow & Metabolism (2009), 1–9

www.jcbfm.com

A novel inhibitor of plasminogen activator inhibitor-1 provides antithrombotic benefits devoid of bleeding effect in nonhuman primates

Yuko Izuhara[1], Nagahisa Yamaoka[2], Hidehiko Kodama[2], Takashi Dan[1], Shunya Takizawa[3], Noriaki Hirayama[4], Kanji Meguro[2], Charles van Ypersele de Strihou[5] and Toshio Miyata[1]

[1]*Center for Translational and Advanced Research, Tohoku University Graduate School of Medicine, Miyagi, Aoba-ku, Sendai, Japan;* [2]*CT Laboratory, Hamari Chemicals Ltd, Osaka, Japan;* [3]*Department of Neurology, Tokai University School of Medicine, Kanagawa, Japan;* [4]*Basic Medical Science and Molecular Medicine, Tokai University School of Medicine, Kanagawa, Japan;* [5]*Service de Nephrologie, Universite Catholique de Louvain, Brussels, Belgium*

Inhibition of plasminogen activator inhibitor (PAI)-1 is useful to treat several disorders including thrombosis. An inhibitor of PAI-1 (TM5275) was newly identified by an extensive study of structure-activity relationship based on a lead compound (TM5007) which was obtained through virtual screening by docking simulations. Its antithrombotic efficacy and adverse effects were tested *in vivo* in rats and nonhuman primates (cynomolgus monkey). TM5275, administered orally in rats (1 to 10 mg/kg), has an antithrombotic effect equivalent to that of ticlopidine (500 mg/kg) in an arterialvenous shunt thrombosis model and to that of clopidogrel (3 mg/kg) in a ferric chloride-treated carotid artery thrombosis model. TM5275 does not modify activated partial thromboplastin time and prothrombin time or platelet activity and does not prolong bleeding time. Combined with tissue plasminogen activator, TM5275 improves the latter's therapeutic efficacy and reduces its adverse effect. Administered to a monkey model of photochemical induced arterial thrombosis, TM5275 (10 mg/kg) has the same antithrombotic effect as clopidogrel (10 mg/kg), without enhanced bleeding. This study documents the antithrombotic benefits of a novel, more powerful, PAI-1 inhibitor in rats and, for the first time, in nonhuman primates. These effects are obtained without adverse effect on bleeding time.
Journal of Cerebral Blood Flow & Metabolism (2009) **0**, 000–000. doi:10.1038/jcbfm.2009.272

Keywords: bleeding; cynomolgus monkey; PAI-1 inhibitor; thrombosis; tissue plasminogen activator

Introduction

Plasminogen activator inhibitor (PAI)-1, a serine protease inhibitor, is involved in numerous processes including thrombosis and fibrosis, as shown by the fact that disruption of the PAI-1 gene in mice markedly attenuates these processes (Carmeliet *et al*, 1993; Eitzman *et al*, 1996, 2000; Weisberg *et al*, 2005; Nicholas *et al*, 2005). Its inhibition may thus yield important cardio- and reno-protective benefits (Ha *et al*, 2009). Recent studies in mice overexpressing human PAI-1 also implicate its involvement in broader biological abnormalities, including alopecia, amyloidosis, and polycystic ovarian syndrome (Eren *et al*, 2007; Devin *et al*, 2007). The availability of specific PAI-1 antagonists may thus open new therapeutic avenues (Vaughan *et al*, 2007).

We have recently developed an original approach to synthesize such orally active inhibitors (Izuhara *et al*, 2008). Compounds selected virtually by structure based drug design underwent a docking simulation to select those which fitted within the cleft of the PAI-1 three-dimensional structure. They inhibit coagulation in two different rodent models of thrombosis and prevent the fibrotic process initiated by bleomycin in mouse lung (Izuhara *et al*, 2008).

This study has been undertaken on a newly synthesized PAI-1 inhibitor (TM5275), to test *in vivo* its antithrombotic efficacy as well as its possible adverse effects. We further assess the clinical benefits of a combination therapy of TM5275 with tissue plasminogen activator (tPA).

Correspondence: Dr T Miyata, Center for Translational and Advanced Research, Tohoku University School of Medicine, 2-1 Seiryo-Machi, Aoba-ku, Sendai 980-8575, Japan.
E-mail: t-miyata@mail.tains.tohoku.ac.jp
Received 7 July 2009; revised 2 December 2009; accepted 9 December 2009

The therapeutic efficacy of TM5275 has been evaluated not only in rodents but also in nonhuman primates as recommended by recent guidelines (STAIR, 1999) to reduce discrepancies between preclinical animal trials and clinical studies. Indeed, the pathophysiological mechanisms involved in the development of thrombosis in preclinical rodent models may differ from those implicated in primates, including man (STAIR, 1999). TM5275 proves an effective antithrombotic agent which spares activated partial thromboplastin time/prothrombin time and platelet activity and does not prolong bleeding time. Combined with tPA, it improves the latter's therapeutic efficacy and reduces its adverse effects.

This study is the first to demonstrate in nonhuman primates that PAI-1 inhibition reduces markedly vascular thrombosis without modification of bleeding time, which is the most critical adverse effect of various antithrombotic agents.

Materials and methods

Synthesis of Test Compounds

More than ninety novel compounds (2-acylamino-3-thiophenecarboxylic acid and 2-acylaminobenzoic acid derivatives with comparatively low molecular weights (400 to 550) and without symmetrical structure, designed based on the original PAI-1 inhibitor TM5007 (Izuhara *et al*, 2008)) as well as PAI-749 (Gardell *et al*, 2007), a previously reported PAI-1 inhibitor, were synthesized by Hamari Chemicals Ltd (Osaka, Japan). They were screened *in vitro* for PAI-1 inhibitory activity.

Docking Simulations

Docking simulations were undertaken by the program ASEDock (Goto *et al*, 2008). The crystal structure of a complex between PAI-1 and the inhibitory reactive-center loop peptide (1A7C) was obtained from the Protein Data Bank (Bernstein *et al*, 1997) and used as the target structure for the docking simulations.

In Vitro PAI-1 Activity Assay

PAI-1 inhibitory activity was assessed by a previously described chromogenic assay (Izuhara *et al*, 2008). The composition of the incubation medium was adapted to increase the assay's sensitivity: 0.15 mol/L NaCl, 50 mmol/L Tris-HCl pH8, 0.2 mmol/L CHAPS, 0.1% PEG-6000, 1% dimethylsulfoxide, 5 nmol/L human active PAI-1, 2 nmol/L human 2-chain tPA and 0.2 mmol/L Spectrozyme tPA at final concentration. Tested compounds were added at various concentrations and the IC_{50} was calculated by logit-log analysis.

PAI-1/tPA Complex on Sodium Dodecyl Sulfate-Polyacrylamide Gel Electrophoresis

The effect of the tested compound on the formation of a PAI-1/tPA complex was estimated in an incubation medium mixing PAI-1, tPA, and the compound. The eventual composition included 100 mmol/L HEPES, pH 7.4, 150 mmol/L NaCl, 0.05% Tween 20, 0.8% dimethylsulfoxide, 0.875 μmol/L PAI-1, 0.7 μmol/L tPA, and compound (160 μmol/L). Proteins were separated by sodium dodecyl sulfate-polyacrylamide gel electrophoresis and visualized by Coomassie staining.

Pharmacokinetic Studies

Animal experiments were performed in accordance with the Animal Experimentation Guidelines of Tokai University School of Medicine. TM5275, suspended in 0.5% carboxymethyl cellulose sodium salt (CMC) solution, was administered orally by gavage to male ICR mice (50 mg/kg) (CLEA Japan Inc., Tokyo, Japan), male Wistar rats (50 mg/kg) (CLEA Japan Inc.), and male cynomolgus monkeys (1 mg/kg) (Macaca Fascicularis) (Japan SLC, Shizuoka, Japan). Heparinized blood samples were collected from the vein before (0 h) and 1, 2, 6, and 24 h after oral drug administration. Plasma drug concentration was determined on a reverse-phase high-performance liquid chromatography. Maximum drug concentration time (T_{max}), maximum drug concentration (C_{max}), and drug half-life ($T_{\frac{1}{2}}$) were then calculated. For the BA study in monkeys, heparinized blood samples were collected from the vein before (0 h) and 0.5, 1, 2, 4, 6, 8, 24, 48, 72, 120, and 168 h after oral drug administration, and before (0 h) and 0.08, 0.25, 0.5, 1, 2, 4, 6, 8, 24, 48, 72, 120, and 168 h after intravenous drug injection. BA was calculated by noncompartment model analysis using WinNonlin Professional Software, version 5.01 (Pharsight Co., NC, USA). Q1

Toxicity

All toxicity studies followed the International Conference on Harmonisation of Technical Requirements for Registration of Pharmaceuticals for Human Use (ICH) Harmonised Tripartite Guidelines at the non-GLP conditions.

For the evaluation of acute toxicity, TM5275 (1000 mg/kg for mice and 2000 mg/kg for rats and monkeys), suspended in 0.5% CMC solution, was administered orally by gavage to male ($n=5$) and female ($n=5$) ICR mice (CLEA Japan Inc.), male ($n=5$) and female ($n=5$) Sprague–Dawley rats (Charles River Japan Inc., Kanagawa, Japan), and male cynomolgus monkeys ($n=2$) (Japan SLC). The animal's body weight was monitored once a week. Various organs underwent histological studies 2 weeks (mice) and 1 week (rats) after drug administration.

For the evaluation of the subacute toxicity, three different doses of TM5275 (200, 600, and 2000 mg/kg/day) were administered for 2 weeks by gavage to male ($n=5$) and female ($n=5$) Sprague–Dawley rats (Charles River Japan) and male cynomolgus monkeys ($n=2$) (Japan SLC). At the end of the study, blood glucose, total cholesterol, triglyceride, aspartate aminotransferase, alanine aminotransferase, creatinine, urea nitrogen, total protein, albumin, hemoglobin, red blood cells, and hematocrit levels as well as activated partial thromboplas-

tin time and prothrombin time were assessed. Body weight was measured and urinary analysis performed.

The following safety pharmacology core battery was used: a modified Irwin's test for the central nervous system in Sprague–Dawley rats dosing TM5275 up to 2 g/kg *per* os, and three cardiovascular tests. (1) QT interval in telemetry electrocardiogram recording in beagle dogs administered an oral dose of 2 g/kg of TM5275; (2) action potentials of guinea-pig right ventricular papillary muscles at a dose of 5 μmol/L of TM5275; and (3) hERGIkr current measured in stably transfected human embryonic kidney (HEK) 293 cells at a dose of 5 μmol/L of TM5275.

Arteriovenous Shunt Thrombosis Rat Model

Thrombus formation in arteriovenous shunts was achieved in male CD rats (Charles River Japan) by a previously described method (Morishima *et al*, 1997). Either TM5275 (10 and 50 mg/kg, $n=9$) or ticlopidine (500 mg/kg, $n=6$: Wako Pure Industries Ltd, Osaka, Japan), suspended in 0.5% CMC solution, was administered orally by gavage 90 mins before the study. Control rats were administered only a 0.5% CMC solution ($n=10$). Blood was allowed to circulate through the shunt for 30 mins. The wet weight of the thrombus covering the silk thread was eventually measured.

Ferric Chloride-Treated Carotid Artery Thrombosis Rat Model

Male Sprague–Dawley rats weighing 280 to 310 g (Japan SLC) were anesthetized with pentobarbital sodium (50 mg/kg, intraperitoneally) and fixed on a heating pad. During the experiment, rectal temperature was maintained at 38°C. The left common carotid artery was exposed, and a piece of filter paper (2.5 × 4.2 mm) was folded around it. The probe of a pulsed Doppler flowmeter (Model PDV-20, Crystal Biotech America, Hopkinton, MA, USA) was placed to measure the arterial blood flow. After obtention of a steady baseline flow, 2 μL of ferric chloride ($FeCl_3$) saline solution (35% (w/w)) was added to the filter paper. Five minutes later, the filter paper was removed and the artery washed with saline. Blood flow in the common carotid artery was continuously monitored for 30 mins after $FeCl_3$ saline exposure. Time to primary occlusion was calculated.

Several concentrations of TM5275 (0.3, 1, 5 mg/kg) and clopidogrel (1, 3, 10 mg/kg) (Sanofi Aventis, Tokyo, Japan), suspended in 0.5% CMC solution, were administered orally by gavage ($n=8$, each group) 2 h before $FeCl_3$ exposure. After a 30 mins blood flow monitoring, a sphygmomanometer cuff was placed on the tail and inflated to 40 mm Hg. An incision was made with an animal lancet (Goldenrod, Medipoint Inc., Mineola, NY, USA) and, every 30 secs, a wick of filtration paper was inserted on the wound until no further staining was observed. Bleeding time was determined to the nearest 30 secs. If it lasted more than 10 mins, the experiment was discontinued.

The benefits of combining TM5275 with tPA were further ascertained. Either TM5275 (5 mg/kg, $n=10$), tPA (0.3 or 3 mg/kg, $n=10$ each: Kyowa Hakko Kirin Co. Ltd), or TM5275 (5 mg/kg) plus tPA (0.3 mg/kg) ($n=10$) were administered orally (TM5275) or intravenously (tPA). The experiments were performed along the conditions described above.

Photochemically Induced Arterial Thrombosis Monkey Model

Three- to 4-year-old male cynomolgus monkeys (Japan SLC) weighing 2.8 to 3.5 kg underwent anesthesia by an intramuscular injection of 10 mg/kg ketamine hydrochloride followed by the intravenous injection of 25 mg/kg pentobarbital sodium. Animals were fixed on a heating pad, and rectal temperature was maintained at 36.5 to 37.5°C. The saphenous artery was exposed by a 2 cm incision and thrombosis was induced by a photochemical reaction according to the modified method of Umemura *et al* (1993). Briefly, the saphenous artery was irradiated with green light (wave length 540 nm, 900,000 lx) generated by a xenon lamp (L4887, Hamamatsu Photonics, Shizuoka, Japan) with a heat-absorbing filter and a green filter. Irradiation was directed by a 3-mm diameter optic fiber mounted on a micromanipulator. The probe of a pulsed Doppler flowmeter (Model PDV-20, Crystal Biotech America) was placed on the saphenous artery to measure arterial blood flow. Once the baseline flow was steady, a 20 mins photo-irradiation was undertaken and a 6 mins intravenous rose bengal (20 mg/kg) injection initiated. TM5275 (10 mg/kg) or clopidogrel (10 mg/kg) suspended in 0.5% CMC solution were administered by gavage ($n=6$, each group) 2 h before photochemical thrombosis. Blood flow of the saphenous artery was monitored for 3 h after the start of photo-irradiation. In monkeys, in contrast with rodents, photochemically induced arterial thrombosis progressively reduced cerebral blood flow, and was followed by recanalization and eventually by rethrombosis, a sequence observed in stroke patients and called cyclical flow reduction (Maeda *et al*, 2005*a*, *b*). Therefore, total occlusion time was calculated during the experiment.

Bleeding time was measured in monkeys previously acclimated to chair restraint during repeated training sessions several times before the experiment. A sphygmomanometer cuff, placed on the upper leg of conscious monkeys fixed to a monkey chair, was inflated to 40 mm Hg. TM5275 (50 mg/kg) or clopidogrel (10 mg/kg) suspended in 0.5% CMC solution were administered orally by gavage ($n=3$, each group) 2 h before the study. Bleeding was produced inside the lower leg by a Micro Lancet (Abbot Japan, Tokyo, Japan) with a 21-gauge needle. Every 10 sec, a wick of filtration paper was placed on the wound until no further staining was observed. Bleeding time was determined to the nearest 10 secs. Maximum observation period was 10 mins.

Statistics

All data are expressed as the mean ± s.e. Comparisons between two groups were performed using an unpaired *t*-test. For multiple comparisons, one-way analysis of

variance and Dunnett's *post hoc* test were performed. The effect of TM5275 combined with tPA in the $FeCl_3$ model was performed by one-way analysis of variance followed by Bonferroni's multiple comparisons. Values are considered significant at $P<0.05$. All statistical analyses were performed on the statistical package SPSS for Windows (Version 15.0, SPSS, Chicago, IL, USA).

Results

TM5275

TM5275, 5-chloro-2-[({2-[4-(diphenylmethyl) piperazin-1-yl]-2-oxoethoxy}acetyl)amino]benzoate (Figure 1B), was discovered through an extensive structure-activity relationship study with more than 90 compounds designed and synthesized on the basis of the structure of TM5007 (Figure 1A). TM5275 was eventually selected as the test compound after taking into consideration the *in vitro* PAI-1 inhibitory activity and pharmacokinetic studies (T_{max}, C_{max}, $T_{\frac{1}{2}}$) (see below).

The PAI-1 inhibitory activity of TM5275, measured by tPA-dependent hydrolysis of peptide substrate, is comparable to that of TM5007 and PAI-749: Half-maximal inhibition (IC_{50}) values of TM5275, TM5007, and PAI-749 are 6.95, 5.60, and 8.37 μmol/L, respectively.

Docking simulation of the PAI-1 moiety and TM5275 was undertaken to understand the mechanism of TM5275 action. TM5275 binds to strand 4 of the A β-sheet (s4A) position of PAI-1. Although both TM5275 and TM5007 bind within the cleft to the s4A segment of PAI-1, closer inspection reveals that their binding sites differ, as illustrated in Figure 2: the bulky diphenylmethyl group of TM5275 cannot be accommodated to the binding site of TM5007, so that TM5275 is markedly shifted in the s4A cleft.

In vitro, TM5275 (up to 100 μmol/L) does not interfere with other serpin/serine protease systems (that is, alpha$_1$-antitrypsin/trypsin and alpha$_2$-antiplasmin/plasmin). Its PAI-1 inhibitory activity thus appears specific. On sodium dodecyl sulfate-polyacrylamide gel electrophoresis, the PAI-1 covalent complex formed with tPA is not observed when PAI-1 is preincubated with TM5275 (data not shown).

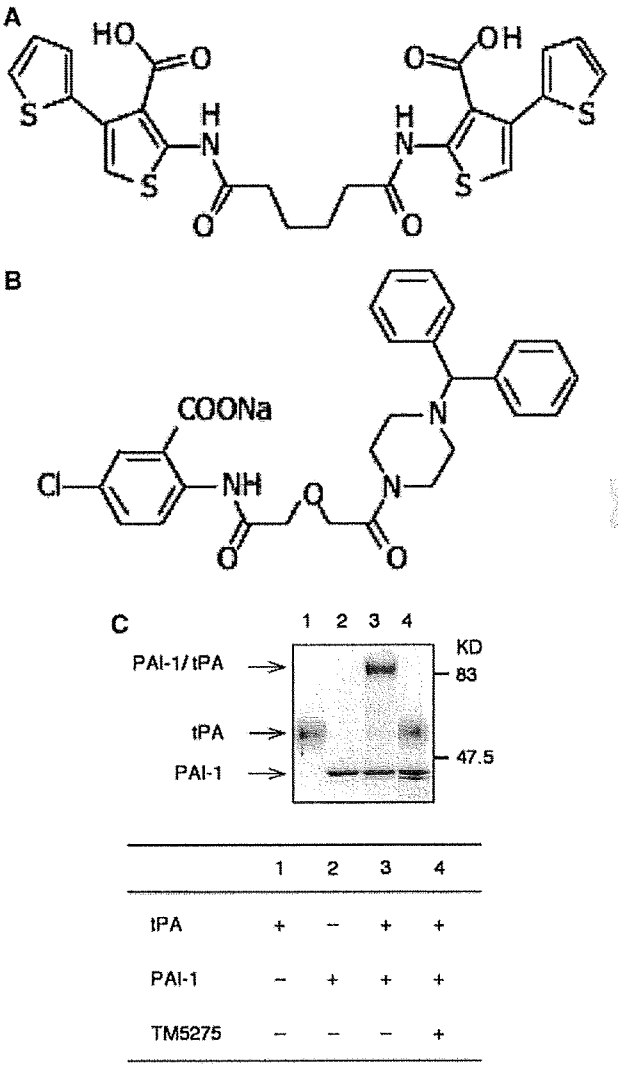

Figure 1 Chemical structures of TM5007 (**A**) and TM5275 (**B**). Molecular weights for TM5007 and TM5275 are 560.02 and 543.97, respectively. On SDS-PAGE (**C**), PAI-1 formed a covalent complex with tPA, whereas no PAI-1/tPA complex formation was observed when PAI-1 was preincubated with TM5275.

Figure 2 The binding modes of TM5007 (cyan) and TM5275 (pink) obtained by docking simulations are shown. Figures were drawn by a software PyMOL version 0.97 (DeLano Scientific LLC, San Carlo, CA, USA).

Pharmacokinetics

The pharmacokinetics of TM5275 improved significantly when compared with that of TM5007. An oral dose of 50 mg/kg of TM5275, administered in rats, yields calculated plasma T_{max}, C_{max}, and $T_{\frac{1}{2}}$ of 2 h, 34 μmol/L, and 2.5 h, respectively, versus 18 h, 8.8 μmol/L, and 124 h, respectively, in rats administered the same dose of TM5007. TM5275 thus increases C_{max} fourfold, and markedly shortens both T_{max} and $T_{\frac{1}{2}}$. In mice, an oral dose of 50 mg/kg of TM5275 yields the following values for these parameters: 1 h, 6.9 μmol/L, and 6.5 h, respectively. In monkeys, an oral dose of 1 mg/kg of TM5275 yields T_{max}, C_{max}, and $T_{\frac{1}{2}}$ values of 6 h, 10.5 μmol/L, and 114.7 h, respectively. Bioavailability of TM5275 reaches 96% in monkeys.

Toxicity

Acute toxicity has been evaluated *in vivo*. A single dose of TM5275 of 1000 mg/kg in mice and 2000 mg/kg in rats and monkeys elicited no symptoms after 2 weeks in the former group and after 1 week in the latter two groups. Body weight and the histology of various organs are not modified.

Subacute toxicity has been assessed in rats and monkeys administered daily three different doses of TM5275 (200, 600, and 2000 mg/kg/day) for 2 weeks. Body weight and the histology of various organs are not modified. No abnormality is noted in the biochemistry of plasma and urine, including activated partial thromboplastin time, prothrombin time, and red blood cell count.

In safety pharmacology studies, TM5275 does not modify tests of the central nervous system (a modified Irwin's test in rats) or of the cardiovascular system: (1) QT interval in electrocardiogram recording in dogs; (2) action potentials of guinea-pig right ventricular papillary muscles; and (3) hERGIkr current in HEK293 cells.

Rat Thrombosis Models

The antithrombotic effectiveness of TM5275 in a rat arteriovenous shunt model is described in Table 1. Blood clot weights are significantly lower in rats administered 10 and 50 mg/kg of TM5275 (60.9 ± 3.0 and 56.8 ± 2.8 mg, respectively) than in vehicle-treated rats (72.5 ± 2.0 mg). Up to 300 mg/kg of TM5007 are needed to reach the efficacy of 50 mg/kg of TM5275 in the same model. The antithrombotic effectiveness of TM5275 (50 mg/kg) is equivalent to that of ticlopidine (500 mg/kg), a reference antithrombotic compound. Plasma concentration of TM5275 reaches 17.5 ± 5.2 μmol/L after a dose of 10 mg/kg.

The antithrombotic effectiveness of TM5275 in a rat $FeCl_3$ carotid artery thrombosis model is illustrated in Figure 3. TM5275 and clopidogrel, another standard antithrombotic drug, prove antithrombotic in a dose-dependent manner (Figure 3). The minimum effective doses of TM5275 and clopidogrel are 1 and 3 mg/kg, respectively. It corresponds to a TM5275 plasma concentration of 4.9 ± 3.6 μmol/L. As expected, clopidogrel prolongs bleeding time in a dose-dependent manner (Figure 3). By contrast, TM5275 does not affect bleeding time, a potential benefit as an antithrombotic agent. Two hours after oral administration, TM5275 (10 mg/kg) does not affect platelet aggregation induced by ADP and collagen (data not shown). Its antithrombotic effect is thus independent of any effect on platelets.

TM5275 has been further combined with tPA in the same model, as illustrated in Figure 4. tPA (0.3 mg/kg) alone does not provide a significant antithrombotic effect. However, TM5275 (5 mg/kg) combined with tPA (0.3 mg/kg) significantly enhances the antithrombotic effect of tPA (0.3 mg/kg) alone and provides a benefit similar to that of a high tPA dose (3 mg/kg). The bleeding time of the combination therapy is similar to that of a low tPA dose (0.3 mg/kg) alone.

Table 1 Effect of TM5275 on thrombus weight in a rat arteriovenous shunt model

Treatment	N	*Thrombus weight subtracting thread (mg)*
Vehicle		
0.5% Carboxymethyl cellulose sodium salt (*per* os)	10	72.5 ± 2.0
TM5275		
10 mg/kg (*per* os)	9	60.9 ± 3.0*
50 mg/kg (*per* os)	9	56.8 ± 2.8†
Ticlopidine		
500 mg/kg (*per* os)	6	51.8 ± 2.2†

Data are expressed as mean ± s.e. *$P < 0.01$, †$P < 0.001$ versus vehicle.

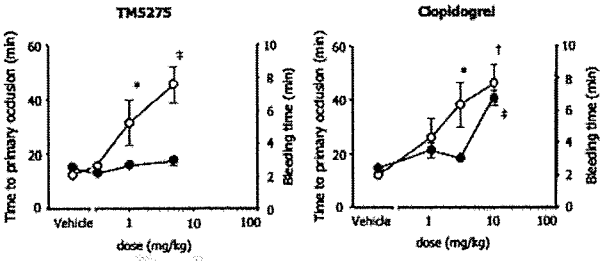

Figure 3 Effects of TM5275 and clopidogrel on primary occlusion time (open circles) and bleeding time (closed circles) in the rat $FeCl_3$-induced thrombosis model. *$P < 0.05$, †$P < 0.01$, ‡$P < 0.001$ versus vehicle. $n = 8$, each group.

Monkey Thrombosis Model

The antithrombotic effect of TM5275 has been evaluated in a cynomolgus monkey model of photo-

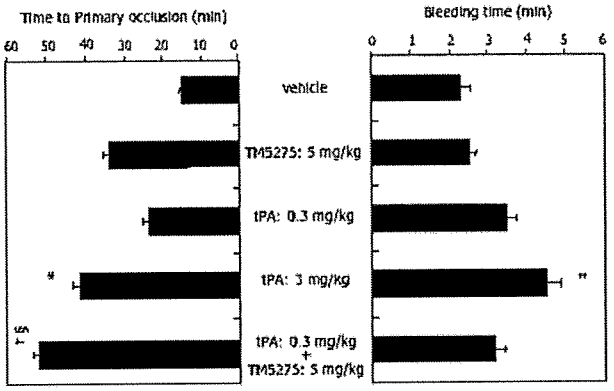

Figure 4 Effect of combination of TM5275 and tPA on primary occlusion time (left panel) and bleeding time (right panel) in the rat $FeCl_3$-induced thrombosis model. $^*P < 0.05$, $^\dagger P < 0.01$, $^\ddagger P < 0.001$ versus vehicle, $^\S P < 0.05$ versus tPA (0.3 mg/kg) alone. $n = 10$, each group.

Table 2 Effect of TM5275 on total occlusion time in the monkey photochemically induced thrombosis model

Treatment	N	*Total occlusion time (min)*
Vehicle 0.5% Carboxymethyl cellulose sodium salt (*per* os)	6	119.0 ± 17.4
Clopidogrel 10 mg/kg (*per* os)	6	39.4 ± 25.8*
TM5275 10 mg/kg (*per* os)	6	53.9 ± 19.9*

Total occlusion time was calculated during the experiment. Data are expressed as mean ± s.e. $^*P < 0.05$ versus vehicle.

chemically induced thrombosis (Table 2). Total occlusion time is significantly reduced in both the TM5275 (53.9 ± 19.9 mins) and clopidogrel (39.4 ± 25.8 mins) groups (10 mg/kg, each) in comparison with the vehicle group (119.0 ± 17.4 mins). Plasma concentration of TM5275 reaches 18.9 ± 3.7 μmol/L in the TM5275 group.

The benefits of TM5275, as an antithrombotic agent devoid of effects on bleeding time, have been confirmed in nonhuman primates (Table 3). Two hours after administration of 50 mg/kg (five times higher than the effective dose) of TM5275, the bleeding time is only slightly longer (146.7 ± 3.3 secs) than before administration (83.3 ± 6.7 secs), whereas it is markedly extended in the 10 mg/kg clopidogrel group (> 600 secs) above that observed before administration (113.3 ± 8.8 secs).

Table 3 Effect of TM5275 on bleeding time in the monkey photochemically induced thrombosis model

Treatment	N	*Bleeding time (secs)*	
		Before administration	*After administration*
Clopidogrel 10 mg/kg (*per* os)	3	113.3 ± 8.8	> 600
TM5275 50 mg/kg (*per* os)	3	83.3 ± 6.7	146.7 ± 3.3

Data are expressed as mean ± s.e.

Discussion

In contrast with a previous rather inefficient high-throughput random screening approach of a large chemical library, we recently reported a novel method to identify small molecular PAI-1 inhibitors, that is, structure-based drug design relying on the virtual screening of small compounds based on the PAI-1 three-dimensional structure (Izuhara *et al*, 2008). Two small molecular PAI-1 inhibitors, TM5001 and TM5007, were thus synthesized and their antithrombotic activity documented in rats (Izuhara *et al*, 2008). In this study, we use the same approach and synthesize a new, more effective PAI-1 inhibitor, TM5275. We show its antithrombotic efficacy not only in rodents but also in monkeys, a more human relevant model.

In limited toxicology studies performed so far, TM5275 appears to be nontoxic. Single doses of 1.0 to 2.0 g/kg elicit no abnormality in rodents or monkeys. Daily doses of 200, 600, or 2000 mg/kg administered for 2 weeks to rats or monkeys also fail to produce symptoms, biochemical disorders, or histological abnormalities in tested organs. More pointed safety pharmacologic tests disclose no neural or cardiovascular toxicity.

Of major interest, TM5275 is 6 times more effective than TM5007: at a dosage of 50 mg/kg, its antithrombotic activity, in a rat arteriovenous shunt model, is equivalent to that obtained by 300 mg/kg of TM5007. This difference is best accounted for by a higher plasma drug concentration of TM5275 reached within 2 h after a 50 mg/kg oral dose, that is, 22.4 μmol/L versus only 5.2 μmol/L after a 300 mg/kg oral dose of TM5007. It fits with the different pharmacokinetic profiles of both drugs: a higher T_{max} reached within a shorter delay after TM5275 (34 μmol/L within 2 h) than after TM5007 (8.8 μmol/L within 18 h). $T_{\frac{1}{2}}$ is more rapid for TM5275 (2.5 h) than for TM5007 (124 h). Interestingly, a lower oral dose of 10 mg/kg administered to nonhuman primates results in intermediary values: T_{max} of 10.5 μmol/L reached within 6 h with a $T_{\frac{1}{2}}$ of 114.7 h. These characteristics argue in favor of oral TM5275 to prevent or dissolve clots in humans, a conclusion further supported by the very high bioavailability of oral TM5275 in monkeys (96%).

Clearly, TM5275 is effective in the prevention of thrombosis in rat models: it dose-dependently

reduces blood clot weight and, at the higher 50 mg/kg doses, is equivalent to a single dose of 500 mg/kg of ticlopidine. In the $FeCl_3$ carotid artery thrombosis model, it (1 mg/kg) also prolongs occlusion time to an extent similar to that of clopidogrel (3 mg/kg) but, unlike the latter, without increasing the bleeding time. In monkeys, the benefits of TM5275 (10 mg/kg) are also apparent as total occlusion time is markedly attenuated to a degree similar to that achieved by clopidogrel (10 mg/kg), but, in contrast to the latter, with only a minor increase in bleeding time.

The differences observed between rodents and monkeys, in TM5275 pharmacokinetics and antithrombotic effects, fully support the recent guidelines (STAIR, 1999) advocating tests in nonhuman primates to reduce discrepancies between preclinical models (usually rodents) and human clinical data. In contrast to rodent thrombosis models, the photochemically induced arterial thrombosis developed in monkeys shows a cyclical flow reduction, that is, a progressive decrease in blood flow with rethrombosis followed by recanalization closely resembling human cerebral thrombosis (Maeda *et al*, 2005*a*, *b*). This difference might reflect specific platelet and coagulation systems. In this nonhuman primate model, TM5275 provides a powerful antithrombotic effect without adverse effects on bleeding time, suggesting its potential benefit, for example, combination therapy with tPA, post-tPA therapy to avoid arterial reocclusion (Alexandrov and Grotta, 2002), treatment for patients with cerebral microbleeds (Nighoghossian *et al*, 2002; Wong *et al*, 2003), or intracranial branch atheromatous disease (Caplan, 1989).

Although tPA has recently become the most effective therapeutic agent for acute ischemic stroke (The National Institute of Neurological Disorders and Stroke rt-PA Stroke Study Group, 1995), symptomatic intracranial hemorrhage remains the most serious, concurrent complication associated with tPA treatment (Derex and Nighoghossian, 2008). In The National Institute of Neurological Disorders and Stroke tPA trial (1995), 6.4% of patients showed a symptomatic intracranial hemorrhage with deterioration of the clinical status in the tPA group, compared with 0.6% in the placebo group. The mortality rate in cases with symptomatic intracranial hemorrhage reached up to 47% (The National Institute of Neurological Disorders and Stroke rt-PA Stroke Study Group, 1997). Recently, an increased risk of intracranial hemorrhage in patients receiving tPA, assessed by concomitant cerebral microbleeding on T2*-weighted magnetic resonance imaging, has been pointed out (Nighoghossian *et al*, 2002), and an alternative thrombolytic therapy without inducing worrisome bleeding disorders often encountered with tPA therapy is expected. We show that, in rats, TM5275 augments its antithrombotic efficacy: added to a standard intravenous dose of tPA (0.3 mg/kg), it more than doubles ($P<0.05$ versus 0.3 mg/kg tPA alone) its time to primary occlusion without increasing bleeding time. Conversely, tPA (3 mg/kg) significantly prolongs the TM5275-induced time to primary occlusion with a small but significant increase in bleeding time. It is noted that the TM5275-tPA (0.3 mg/kg) combination, compared with a 10 times higher dose of injected tPA (3 mg/kg), achieves a longer time to primary occlusion ($P<0.01$ versus vehicle) with a decreased bleeding time. These data obtained in rats suggest that an appropriate combination of oral TM5275 with intravenous tPA might prove valuable in clinical emergencies without inducing worrisome bleeding disorders.

Clinical deterioration after tPA therapy was observed in the National Institute of Neurological Disorders and Stroke rt-PA Stroke Study (Grotta *et al*, 2001), and early cerebral arterial reocclusion occurs in 34% of tPA-treated patients with any initial recanalization (Alexandrov and Grotta, 2002). Oral administration of TM5275, followed by intravenous tPA treatment, may be beneficial. Also, the presence of cerebral microbleeds on T2*-weighted magnetic resonance imaging has been pointed out as a marker of increased risk of intracranial hemorrhage in patients receiving tPA (Nighoghossian *et al*, 2002) or taking aspirin (Wong *et al*, 2003). An alternative thrombolytic and/or antiplatelet therapy without inducing worrisome bleeding disorders, such as TM5275, may therefore provide benefits. Q3

Intracranial branch atheromatous disease is another candidate for TM5275 treatment. Patients with atheromatous disease of an arterial branch present a gradual or stepwise progression of clinical signs, because platelet-fibrin plugs may form, break off, and embolize distally (Caplan, 1989), a mechanism mimicking the cyclical flow reduction by the photochemically induced arterial thrombosis (Maeda *et al*, 2005*a*, *b*) shown in our study using cynomolgus monkeys.

Several characteristics of TM5275 might prove helpful in the treatment of thrombotic disorders. First of all, unlike other types of antithrombotic agents for example, anticoagulation or antiplatelet agents), it does not prolong bleeding time and has virtually no influence on activated partial thromboplastin time/prothrombin time and platelet activity. Second, its impressive bioavailability warrants an administration *per* os, a substantial advantage over tPA. The demonstration that, combined with the latter, it enhances its activity supports a joint administration.

It is noteworthy that inhibition of PAI-1 in humans may not induce serious adverse effects. Currently, two genetic defects in the PAI-1 gene have been documented in humans (Mehta and Shapiro, 2008). Affected individuals do have a mild bleeding tendency but rarely exhibit severe bleeding events commonly seen in other procoagulant deficiencies: most episodes are post-traumatic or post-surgical. The majority of bleeding events are controlled with

antifibrinolytic agents, such as tranexamic acid and ε-aminocaproic acid. In PAI-1-deficient patients, a normal lifespan is achieved. Further clinical studies are needed to support these conclusions.

Acknowledgements

This study was supported by a grant from the New Energy and Industrial Technology Development Organization in Japan (to TM and NH).

Conflict of interest

The authors declare no conflict of interest.

References

Alexandrov AV, Grotta JC (2002) Arterial reocclusion in stroke patients treated with intravenous tissue plasminogen activator. *Neurology* 59:862–7

Bernstein FC, Koetzle TF, Williams GJ, Meyer EF, Jr, Brice MD, Rodgers JR, Kennard O, Shimanouchi T, Tasumi M (1997) The protein data bank: a computer-based archival file for macromolecular structures. *J Mol Biol* 112:535–42

Caplan LR (1989) Intracranial branch atheromatous disease: a neglected, understudied, and underused concept. *Neurology* 39:1246–50

Carmeliet P, Stassen JM, Schoonjans L, Ream B, van den Oord JJ, De Mol M, Mulligan RC, Collen D (1993) Plasminogen activator inhibitor-1 gene-deficient mice: II Effects on hemostasis, thrombosis, and thrombolysis. *J Clin Invest* 92:2756–60

Derex L, Nighoghossian N (2008) Intracerebral haemorrhage after thrombolysis for acute ischaemic stroke: an update. *J Neurol Neurosurg Psychiatry* 79:1093–9

Devin JK, Johnson JE, Eren M, Gleaves LA, Bradham WS, Bloodworth JR, Jr, Vaughan DE (2007) Transgenic overexpression of plasminogen activator inhibitor-1 promotes the development of polycystic ovarian changes in female mice. *J Mol Endocrinol* 39:9–16

Eitzman DT, McCoy RD, Zheng X, Fay WP, Shen T, Ginsburg D, Simon RH (1996) Bleomycin-induced pulmonary fibrosis in transgenic mice that either lack or overexpress the murine plasminogen activator inhibitor-1 gene. *J Clin Invest* 97:232–7

Eitzman DT, Westrick RJ, Xu Z, Tyson J, Ginsburg D (2000) Plasminogen activator inhibitor-1 deficiency protects against atherosclerosis progression in the mouse carotid artery. *Blood* 96:4212–5

Eren M, Gleaves LA, Atkinson JB, King LE, Declerck PJ, Vaughan DE (2007) Reactive site-dependent phenotypic alterations in plasminogen activator inhibitor-1 transgenic mice. *J Thromb Haemost* 5:1500–8

Gardell SJ, Krueger JA, Antrilli TA, Elokdah H, Mayer S, Orcutt SJ, Crandall DL, Vlasuk GP (2007) Neutralization of plasminogen activator inhibitor 1 (PAI-1) by the synthetic antagonist PAI-749 via a dual mechanism of action. *Mol Pharmacol* 72:897–906

Goto J, Kataoka R, Muta H, Hirayama N (2008) ASEDock-docking based on alpha spheres and excluded volumes. *J Chem Inf Model* 48:583–90

Grotta JC, Welch KM, Fagan SC, Lu M, Frankel MR, Brott T, Levine SR, Lyden PD (2001) Clinical deterioration following improvement in the NINDS rt-PA Stroke Trial. *Stroke* 32:661–8

Ha H, Oh EY, Lee HB (2009) The role of plasminogen activator inhibitor 1 in renal and cardiovascular diseases. *Nat Rev Nephrol* 5:203–11

Izuhara Y, Takahashi S, Nangaku M, Takizawa S, Ishida H, Kurokawa K, van Ypersele de Strihou C, Hirayama N, Miyata T (2008) Inhibition of plasminogen activator inhibitor-1: its mechanism and effectiveness on coagulation and fibrosis. *Arterioscler Thromb Vasc Biol* 28:672–7

Maeda M, Moriguchi A, Mihara K, Aoki T, Takamatsu H, Matsuoka N, Mutoh S, Goto T (2005a) FK419, a nonpeptide platelet glycoprotein IIb/IIIa antagonist, ameliorates brain infarction associated with thrombotic focal cerebral ischemia in monkeys: comparison with tissue plasminogen activator. *J Cereb Blood Flow Metab* 25:108–18

Maeda M, Takamatsu H, Furuichi Y, Noda A, Awaga Y, Tatsumi M, Yamamoto M, Ichise R, Nishimura S, Matsuoka N (2005b) Characterization of a novel thrombotic middle cerebral artery occlusion model in monkeys that exhibits progressive hypoperfusion and robust cortical infarction. *J Neurosci Methods* 146:106–15

Mehta R, Shapiro AD (2008) Plasminogen activator inhibitor type 1 deficiency. *Haemophilia* 14: 1255–60

Morishima Y, Tanabe K, Terada Y, Hara T, Kunitada S (1997) Antithrombotic and hemorrhagic effects of DX-9065a, a direct and selective factor Xa inhibitor: comparison with a direct thrombin inhibitor and antithombin III-dependent anticoagulants. *Thromb Haemost* 78:1366–71

Nicholas SB, Aguiniga E, Ren Y, Kim J, Wong J, Govindarajan N, Noda M, Wang W, Kawano Y, Collins A, Hsueh WA (2005) Plasminogen activator inhibitor-1 deficiency retards diabetic nephropathy. *Kidney Int* 67:1297–307

Nighoghossian N, Hermier M, Adeleine P, Blanc-Lasserre K, Derex L, Honnorat J, Philippeau F, Dugor JF, Froment JC, Trouillas P (2002) Old microbleeds are a potential risk factor for cerebral bleeding after ischemic stroke: a gradient–echo T2*-weighted brain MRI study. *Stroke* 33:735–42

Stroke Therapy Academic Industry Roundtable (STAIR) (1999) Recommendations for standards regarding preclinical neuroprotective and restorative drug development. *Stroke* 30:2752–8

The National Institute of Neurological Disorders and Stroke rt-PA Stroke Study Group (1995) Tissue plasminogen activator for acute ischemic stroke. *N Engl J Med* 333:1581–7

The National Institute of Neurological Disorders and Stroke rt-PA Stroke Study Group (1997) Intracerebral hemorrhage after intravenous t-PA therapy for ischemic stroke. The NINDS t-PA Stroke Study Group. *Stroke* 28:2109–18

Umemura K, Wada K, Uematsu T, Nakashima M (1993) Evaluation of the combination of a tissue-type plasminogen activator, SUN9216, and a thromboxane A2 receptor antagonist, vapiprost, in a rat middle cerebral artery thrombosis model. *Stroke* 24: 1077–1082

Vaughan DE, De Taeye BM, Eren M (2007) PAI-1 antagonists: predictable indications and unconventional applications. *Curr Drug Targets* 8:962–70

Weisberg AD, Albornoz F, Griffin JP, Crandall DL, Elokdah H, Fogo AB, Vaughan DE, Brown NJ (2005) Pharmacological inhibition and genetic deficiency of plasminogen activator inhibitor-1 attenuates angiotensin II/salt-induced aortic remodeling. *Arterioscler Thromb Vasc Biol* 25:365–71

Wong KS, Chan YL, Liu JY, Gao S, Lam WW (2003) Asymptomatic microbleeds as a risk factor for aspirin-associated intracerebral hemorrhages. *Neurology* 60:511–3

///// Cutting Edge /////

擬似分子プローブと標的分子構造に基づく *de novo* 医薬分子設計法の開発

東田欣也[1]、後藤純一[1]、平山令明[2]
1. 株式会社菱化システム科学技術システム事業部計算科学部
2. 東海大学医学部

1. はじめに

医薬分子の *de novo* デザイン手法の一つに、標的分子（多くの場合はタンパク質）との結合に深く関与する原子団（以下反応原子団）を含む部分化学構造をつなぎ合わせて新規仮想分子を構築する方法がある。しかし、部分化学構造とそれらを連結する化学構造（リンカー）を機械的に組み合わせると、膨大な仮想分子が発生してしまう。そこで、標的分子の構造情報を最大限に活用し、かつ標的分子への親和性の高い仮想分子を発生させる強力なアルゴリズムが必要になる。このようなコンセプトで作られたアルゴリズムが現在ない訳ではないが、その殆どが実用性という観点から必ずしも満足のいくものではなく、より強力なアルゴリズムの開発が望まれてきた。

さて、X線解析等で得られた標的分子の結合部位情報に基づいて、その部位に結合できる新規の分子をデザインする場合、まず決定すべきことは、結合部位内に配置すべき反応原子団の位置である。この作業が*de novo*デザインにおいて、最も重要であり、かつ最も難しいステップでもある。我々は、この作業を合理的かつ能率的に遂行するために、擬似分子プローブという新しいコンセプトを用いた*de novo*医薬分子デザインのアルゴリズムであるPseudo Molecular Probe (PMP) 法を開発した[1]。

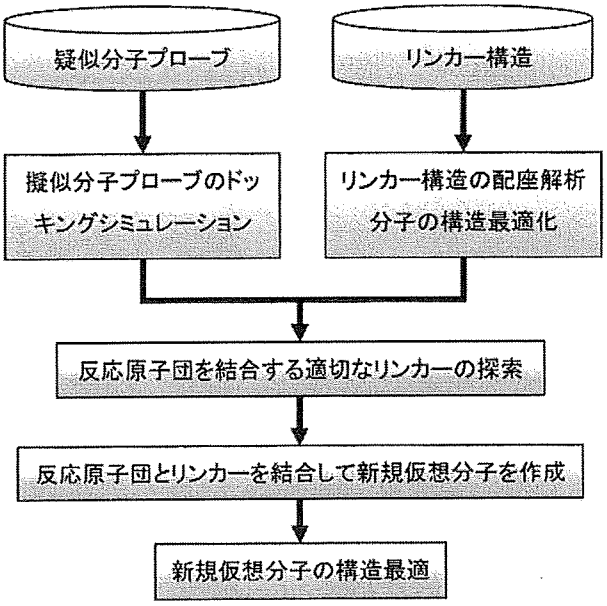

図1　PMP法のフローチャート

2. 方法

2.1. 手順の概要

今回開発した新規 *de novo* 分子デザイン法である PMP 法の手順を図 1 に示す。まず初めに、反応原子団を有する擬似分子プローブをタンパク質の結合部位内の適切な位置にドッキングシミュレーションにより配置する。リンカーに用いる化学構造の可能な立体配座は、予め配座解析により発生しておく。仮想分子は、擬似分子プローブとリンカーを両者の特定の非水素原子位置で重ね合わせることで構築するが、それらの原子位置を結合点と呼ぶことにする。擬似分子プローブの結合点は原則として 1 箇所であるが、リンカー構造については結合点が複数存在する場合もある。そこで、可能な配置を網羅的に探索し、擬似分子プローブとリンカーの結合点を結合した仮想分子を全て作成する。最終的に、タンパク質の結合部位で仮想分子の構造最適化を行うことにより、タンパク質との結合性が高い仮想分子を選択する。

2.2. 擬似分子プローブの作成

標的分子に対する結合性が高い反応原子団の結合部位における適切な配置を探索するために、擬似分子プローブという新しいコンセプトを本研究では導入した。本研究により、*de novo* 分子デザインを実現する上で、シクロプロペニルメチル（CPM）基を反応原子団に結合させた擬似分子プローブ（図 2）を用いることが有用であると確認できた。

本アルゴリズム検証のために PDB[2]から 4 種の医薬分子とその標的分子との複合体 X 線構造を選択した。1GKC、1KE5、1OTH および 1T46 である。各構造中のリガンドとそれに基づき作成した擬似分子プローブを表 1 に示す。

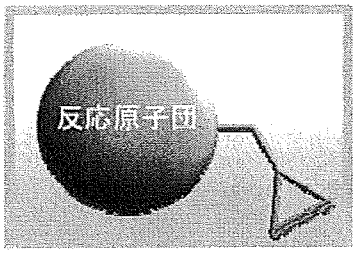

図 2 疑似分子プローブ

PDB コード	リガンド	擬似分子プローブ
1GKC	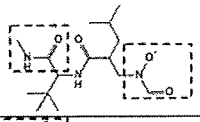	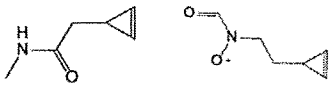
1KE5	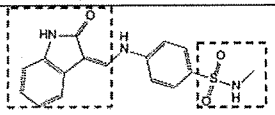	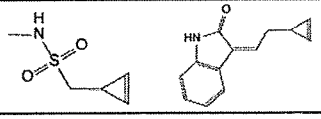
1OTH	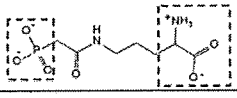	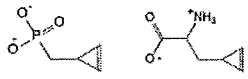
1T46	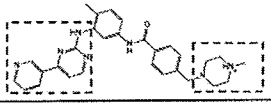	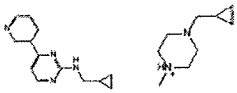

表 1 リガンドから作成した疑似分子プローブ
破線で囲んだ部分は擬似分子プローブに用いた反応原子団

2.3. 擬似分子プローブの結合部位への配置

タンパク質表面の結合部位の検出には、MOE[3] (Molecular Operating Environment) の Site Finder プログラムを用いた。Site Finder は、アルファ球と呼ばれる小球を標的分子の 4 つの重原子に接する位置に置き、そのアルファ球のクラスタ（アルファサイト）によりリガンド結合部位の形状、大きさ、親

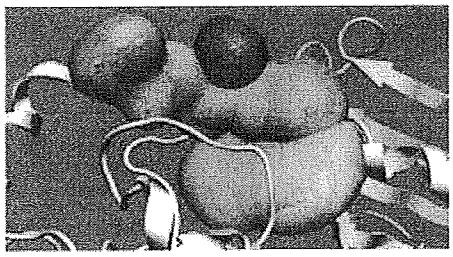

図 3 重複分割した 1OTH の結合部位

水性／疎水性領域の分布を表現する。しかし、Site Finder で求められるアルファサイトは結合部位全体を反映するため、擬似分子プローブの結合部位を求める上では必ずしも適切ではなかった。そこで本研究では、疑似分子プローブの結合部位として妥当な大きさになるように、擬似分子プローブと同程度の体積に、アルファサイトを重複分割した（図 3）。

結合部位における擬似分子プローブの結合性および結合位置はドッキング法（MOE-ASEDock[4]）により決定した。CPM 基の立体的な効果により、反応原子団はタンパク質側に配向し、CPM 基は結合部位の空洞側に配向する。即ち、CPM 基が本来のリガンドの母核構造に代わる働きをしている。実際に擬似分子プローブだけのドッキングでも、反応原子団は X 線結晶構造に近い位置に配置することができた。

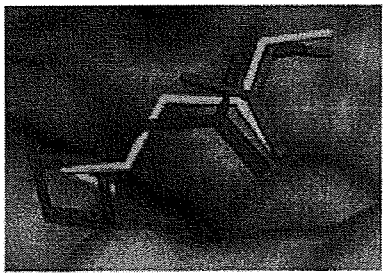

図 4 反応原子団に CPM 基または CBM 基を付加した擬似分子プローブの比較（1GKC）　赤：X 線結晶構造、緑：CPM 基を付加した擬似分子プローブ、青：CBM 基を付加した擬似分子プローブ

なお、CPM 基を持たない構造では、反応原子団の可動範囲が広くなりすぎて、X 線結晶構造とは異なる配置しか得られなかった。さらに、メチレンを除いたシクロプロペニル基や 4 員環を持つシクロブタジエニルメチル（CBM）基を用いると、それらの立体効果の影響で適切に反応原子団を配置できない場合が生じる（図 4）。

2.4. 適切なリンカー配座の検出

擬似分子プローブとリンカーを用いた仮想分子の構築は、両者の二つの非水素原子を重ね合わせることで実現した。CPM 基のメチレン炭素原子を第二結合点とし、その原子に直接結合した反応原子団の非水素原子を第一結合点とする。リンカー構造は、1 つ以上の水素原子を持つ全ての非水素原子を第一結合点とし、第一結合点から水素原子の方向へ 1.5 Å離れた点を第二結合点とした（図 5）。擬似分子プローブおよびリンカー構造の対応する第一結合点と第二結合点の重なりの誤差の許容値は、各々0.2 および 0.3 Å として、新規仮想分子を構築した。

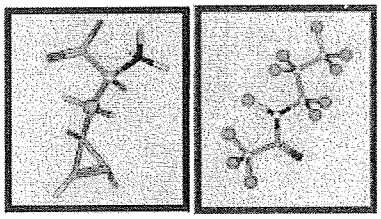

図 5 擬似分子プローブとリンカー構造の結合点　青枠：擬似分子プローブ、赤枠：リンカー構造、黄球：第一結合点、緑球：第二結合点

リンカー構造の候補構造には元のリガンド分子から反応原子団を除いた構造も考慮し、さらにその構造と同程度の体積を持つリンカー構造を DCUJ[5]から選択して、候補構造に加えた。1GKC、1KE5、1OTH および 1T46 に対して用いたリンカー構造は各々113、19、20 および 139 種類である。これらのリンカー構造の可能な立体配座は、MOE-Conformation Import 機能を用いて発生させた。擬似分子プローブに用いた反応原子団は、元のリガンド中に存在している反応原子団のみを採用した。

2.5. 構造最適化とドッキングスコア

MMFF94x 力場を用い、タンパク質の結合部位内で各仮想分子の構造最適化を行った。仮想分子の標的タンパク質分子に対する結合性は次の U_{dock} により評価した。

$$U_{dock} = U_{ele} + U_{vdw} + U_{strain}$$

ここで U_{ele} はタンパク質－仮想分子間の静電相互作用エネルギー、U_{vdw} は同 van der Waals 相互作用エネルギー、U_{strain} は仮想分子のドッキング構造とドッキング構造から最も近い極小構造のポテンシャルエネルギーの差である。

3. 結果

表 2 の「仮想分子の配座数」は、PMP 法により生成した仮想分子のドッキング構造の数である。「U_{dock} の最小値」は、ドッキング構造中の最小 U_{dock} 値を示す。得られた仮想分子の種類は、1GKC、1KE5、1OTH および 1T46 に対して各々3384、111、254 および 4519 だった。

1OTH では U_{dock} による評価が最も良好な分子が実際のリガンドであった、その構造と X 線結晶構造との RMSD（対応する非水素原子位置に関する root mean square deviation）は 1.13Å であり、この場合は PMP 法によって、良好に分子が構築できたことを示す。1GKC、1KE5 では、U_{dock} 値についてそれぞれ第 65 位および 61 位の構造が X 線結晶構造と最も近く、それらの RMSD も十分小さな値だった。一方、1T46 ではかなりの数の配座が得られたにも関わらず、今回の計算条件では X 線結晶構造と同じ分子は得られなかった。しかし、擬似分子プローブの第一結合点における一致許容範囲を今回採用した 0.2Å から 0.3Å に広げれば、この構造についても X 線結晶構造に近い仮想分子を得ることができた。しかし結合点の一致許容範囲を 0.3Å に広げることにより、多くの無意味と思われる構造が生成され、適切な仮想分子の選択が困難になった。

PDB コード	リンカー構造の数	仮想分子の配座数	U_{dock} の最小値 (kcal/mol)	X 線結晶構造に最も近い配座の U_{dock} (kcal/mol)	X 線結晶構造に最も近い配座の順位（U_{dock} 値）	X 線結晶構造との RMSD (Å)
1GKC	113	9113	-185.3	-157.8	65	1.08
1KE5	19	250	-89.38	-43.69	61	1.31
1OTH	20	989	-377.2	-377.2	1	1.13
1T46	137	11527	-107.6	-	-	-

表 2　PMP 法による計算結果

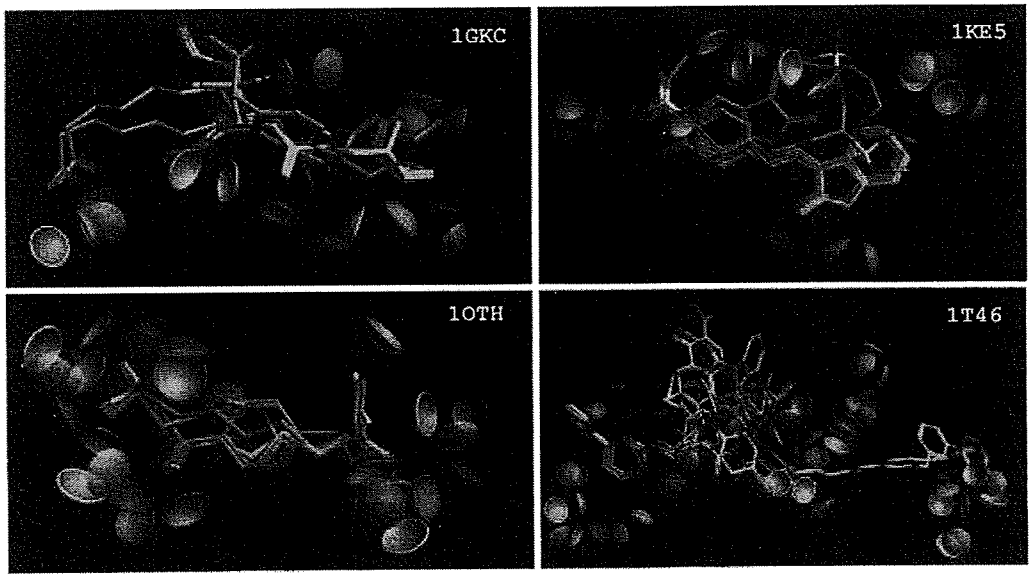

図 6　PMP 法で得られた主な化合物のドッキング構造　緑の構造は X 線結晶構造、元素で色分けした構造は PMP 法で作られた構造。紫、青の傘はそれぞれタンパク質の水素結合ドナーまたはアクセプター原子からの影響を示す。

4. 考察

新しい概念である擬似分子プローブを用いた *de novo* 分子デザイン法である PMP 法を開発し、その機能を 4 種類の標的分子に対して適用した。今回の評価では、既知のリガンドが、そのリガンドの部分化学構造を含む複数の構造断片から再構築でき、かつ標的分子の位置に X 線構造に匹敵する正確さで結合できるかどうかを検証した。一方、複合体構造中に含まれる分子が最適の

リガンドであるという保証がないので、PMP 法で得られる最良の解が X 線構造に一致することは担保されている訳ではない。また、PMP 法は、本来結合性の高い仮想分子を発生するため、これら未合成の仮想分子の中に結合性のより高いものが含まれている可能性は十分ある。しかし、今回の検証で、1OTH に関しては最終的なドッキングにより最も結合性が高いと判断された仮想分子が実際のリガンドと一致し、その配置まで正確に決定することができた。1GKC および 1KE5 でも、結合性の高い分子として得られた仮想分子の結合性上位に実際のリガンドと一致する分子が含まれていた。この 3 例を見る限り、PMP 法は十分に実用的であり、新規分子の設計を標的分子の構造のみから求める上で有用であることを示している。

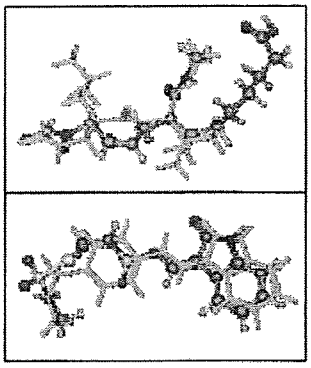

図 7　既知リガンドと異なりかつ U_{dock} がより良好な仮想分子　上段：1GKC、下段：1KE5、棒モデル：X 線結晶構造、棒球モデル：仮想分子

1T46 については今回用いたプロトコルでは、複合体中に含まれるリガンドに一致する仮想分子を生成することはできなかった。しかし、擬似分子プローブとリンカー構造の結合点の一致許容範囲を大きくすると、発生する配座数が増加するが、複合体 X 線構造中に存在するリガンド構造を発生することができた。4 分子の中で、1T46 のリガンドが最も分子サイズが大きく、かつ自由度が大きい。今回検討したプロトコルでは、この系を考慮することができなかったが、これは PMP 法の本質的な限界というより、計算条件の最適化が不十分である可能性が高く、今後 PMP 法を改良することで乗り越えることのできる課題であると考える。

水分子をプローブに用いてタンパク質表面を解析し、他分子との相互作用に関与する部位を探索することは広く行われている。そうした例には、溶媒露出表面とエピトープ性の相関解析などがある。本研究で新しく導入した擬似分子プローブの概念は、分子表面をプローブ分子で探索するという意味で、水分子プローブの拡張概念である。標的分子の表面を可能な限り精査し、そこからの影響を敏感に感じるためには、適切な化学構造を擬似分子プローブに採用しなければならない。すなわち、適切な擬似分子プローブを採用することで、我々は標的分子の表面を正確に探ることも可能である。本研究で種々の擬似分子プローブを試みた結果、シクロペンチルメチル基を複数の反応原子団に結合させたプローブが非常に有効に機能することが見出された。この擬似分子プローブの特徴は、反応原子団が効果的に標的分子の結合部位にある化学的および構造的な特徴を探査できることにある。本研究の結果は、擬似分子プローブの活用が標的分子に対する新規リガンドの発見に有用なだけでなく、様々な生体高分子の機能解析にも有効であることを強く示唆するものである。

5. 謝辞

第 36 回構造活性相関シンポジウムの発表において、貴重なご意見、ご指導を賜りました多くの先生方に心よりお礼申し上げます。本研究内容を本誌に掲載して頂く機会を与えてくださいました諸先生方に心よりお礼申し上げます。

6. 参考文献

(1) K.Toda, J.Goto and N.Hirayama *J. Chem. Inf. Model.*, to be submitted.
(2) H.M. Berman, J. Westbrook, Z. Feng, G. Gilliland, T.N. Bhat, H. Weissig, I.N. Shindyalov, P.E. Bourne *Nucleic Acids Research*, **2000**, *28*, 235-242.
(3) MOE (Molecular Operating Environment), Version 2007.0902; Chemical Computing Group Inc.: Montreal, Quebec, Canada **2007**.
(4) J. Goto, R. Kataoka, H. Muta and N. Hirayama *J. Chem. Inf. Model.*, **2008**, *48*, 583-590.
(5) K. Horio, H. Muta, J. Goto and N. Hirayama *Chem. Pharm. Bull.*, **2007**, *55*, 980-984.

Acta Crystallographica Section F
Structural Biology and Crystallization Communications
ISSN 1744-3091

Daisuke Nakayama, Youssef Ben Ammar and Soichi Takeda*

Department of Cardiac Physiology, National Cardiovascular Center Research Institute, Japan

Correspondence e-mail: stakeda@ri.ncvc.go.jp

Received 7 October 2009
Accepted 5 November 2009

Crystallization and preliminary X-ray crystallographic analysis of blood coagulation factor V-activating proteinase (RVV-V) from Russell's viper venom

Russell's viper venom blood coagulation factor V activator (RVV-V) is a thrombin-like serine proteinase that specifically activates factor V by cleaving a single peptide bond between Arg1545 and Ser1546. Activated factor V combines with activated factor X produced by the enzyme RVV-X in the venom to form the prothombinase complex, which can induce disseminated intravascular coagulopathy in envenomated animals. In the current study, RVV-V was crystallized in order to attempt to understand its substrate specificity for factor V. Four distinct crystal forms of RVV-V were obtained using the sitting-drop vapour-diffusion method and diffraction data sets were collected on SPring-8 beamlines. The best crystal of RVV-V generated data sets to 1.9 Å resolution.

1. Introduction

Blood coagulation factor V is a key component of the haemostatic system (Nicolaes & Dahlback, 2002). Factor V exists as a precursor molecule in the circulation and is converted to its active form, factor Va, after cleavage of the three peptide bonds between Arg709 and Ser710, between Arg1018 and Thr1019 and between Arg1545 and Ser1546 by thrombin or activated factor X (factor Xa; Mann & Kalafatis, 2003; Thorelli *et al.*, 1998). Factor Va acts as a nonenzymatic cofactor in the prothrombinase complex that converts prothrombin to thrombin. Factor Va also enhances the rate of prothrombin activation of factor Xa on phospholipid membranes. This rate is enhanced by about 300 000-fold and enhancement occurs in a Ca^{2+}-dependent manner (Nesheim *et al.*, 1979; Rosing *et al.*, 1980). Finally, thrombin converts soluble fibrinogen into insoluble fibrin, leading to blood-clot formation.

The venom of Russell's viper (*Daboia russelli siamensis*) has been recognized for its potent coagulation activity. Two major components of Russell's viper venom can collaboratively accelerate disseminated intravascular coagulation in the body of prey (Schiffman *et al.*, 1969). One of these components is RVV-X (EC 3.4.24.58), a heterotrimeric metalloproteinase that specifically activates factor X. We recently determined the crystal structure of RVV-X at 2.9 Å resolution and proposed a model for factor-X activation (Takeda *et al.*, 2007). The other component is RVV-V (EC 3.4.21.95), a thrombin-like serine proteinase that specifically activates factor V (Hjort, 1957). RVV-V cleaves the single peptide bond between Arg1545 and Ser1546, resulting in activation of factor V (Dahlback, 1986; Kane & Davie, 1986, 1988; Jenny *et al.*, 1987). RVV-V does not cleave the other two thrombin-susceptible sites of factor V. Furthermore, RVV-V is resistant to endogenous serine proteinase inhibitors (serpins) such as antithrombin, which regulates thrombin activity under physiological conditions (Segers *et al.*, 2006).

The molecular mechanism by which RVV-V recognizes and cleaves the Arg1545–Ser1546 bond of factor V is poorly understood, primarily owing to a lack of high-resolution structural information, although a homology model of RVV-V has previously been reported (Segers *et al.*, 2006). To gain insight into the molecular basis of its substrate recognition and serpin resistance, we crystallographically analyzed RVV-V. Here, we report the crystallization and preliminary crystallographic studies of RVV-V with and without inhibitors.

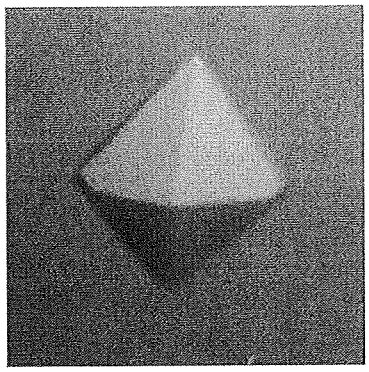

2. Materials and methods

2.1. Purification

D. russelli siamensis venom was purchased from the Japan Snake Institute. RVV-V was purified as described previously (Schiffman *et al.*, 1969; Kisiel, 1979) with some modifications. Lyophilized crude venom powder (200 mg) was dissolved in TBS buffer (10 m*M* Tris–HCl pH 7.5 and 150 m*M* NaCl) to a final concentration of 40 mg ml^{-1} and centrifuged at 15 000*g* for 30 min. The supernatant was loaded onto a HiPrep 26/60 Sephacryl S-100 HR column (GE Healthcare, UK) equilibrated with TBS buffer. Fractions containing RVV-V were pooled and applied onto a 1 ml Resource S column (GE Healthcare) pre-equilibrated with TBS buffer. Nonspecifically bound proteins were eluted with washing buffer (10 m*M* Tris–HCl pH 7.5 and 200 m*M* NaCl pH 7.5) and bound proteins were eluted with a linear gradient of NaCl (200–600 m*M*) in 10 m*M* Tris–HCl pH 7.5. The fractions containing RVV-V were pooled, dialyzed against 10 m*M* Tris–HCl, concentrated using Vivaspin (Sartorius, Germany) with a 10 000 nominal molecular-weight-limit membrane to give a protein concentration of 11.3 mg ml^{-1} and subjected to crystallization.

2.2. Crystallization

Preliminary screening of the crystallization conditions was performed with PEG/Ion 1, PEG/Ion 2, Crystal Screen 1 and Crystal Screen 2 kits (Hampton Research, USA) using the sitting-drop vapour-diffusion method at 277 and 293 K. Protein aliquots (0.1 µl at a concentration of 11.3 mg ml^{-1}) with or without the inhibitors Pefabloc [4-(2-aminoethyl)-benzenesulfonyl fluoride; 10 m*M*; Roche, Switzerland] or PPACK (D-Phe-Pro-Arg-chloromethylketone; 10 m*M*; Calbiochem, Germany) were mixed with 0.1 µl reservoir solution using a repeatable nanolitre pipetting device (Mosquito, TTP Labotech, UK). Droplets were equilibrated against 100 µl reservoir solution.

2.3. Crystallographic data collection

For X-ray measurements, crystals were cryoprotected, mounted in a nylon loop (Hampton Research, USA) or a Lytho Loop (Protein-Wave Corp., Japan) and immediately exposed to a stream of nitrogen gas at 100 K to flash-freeze the samples. The crystals were evaluated in-house using Cu $K\alpha$ radiation (λ = 1.5418 Å) generated by an RA-Micro 7 rotating-anode X-ray generator with an R-AXIS VII image-plate detector (Rigaku, Japan). High-resolution data sets were collected using a Rayonix MX225HE CCD detector installed on the BL41XU beamline at SPring-8. The images collected were processed using the *HKL*-2000 software (Otwinowski & Minor, 1997).

3. Results and discussion

3.1. Purification

RVV-V was purified from the crude venom of *D. russelli siamensis* using gel-filtration chromatography followed by cation-exchange chromatography. The homogeneity of the purified RVV-V was confirmed by SDS–PAGE in the presence or absence of 10 m*M* dithiothreitol (Laemmli, 1970). RVV-V consists of 236 amino acids with a molecular weight of 29 kDa (Tokunaga *et al.*, 1988). Consistent with this previous report, after two-step chromatography the purified RVV-V band was detected at about 29 kDa (Fig. 1). Approximately 4 mg RVV-V was purified from 200 mg crude venom.

3.2. Crystallization

RVV-V crystals were initially obtained under two distinct conditions. Form 1 crystals were obtained using solution No. 38 of the PEG/Ion 2 kit [50 m*M* citric acid, 50 m*M* bis-tris propane pH 5.0 and 20%(*w*/*v*) PEG 3350] at 293 K. Form 2 crystals were obtained using solution No. 47 of the PEG/Ion 2 kit [1%(*w*/*v*) tryptone, 0.05 *M* Na HEPES pH 7.0 and 12%(*w*/*v*) PEG 3350] at 293 K. Crystals of

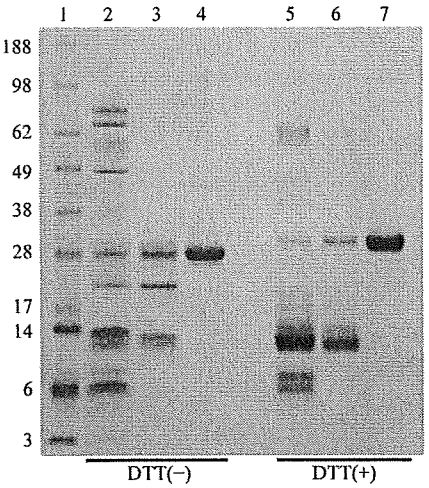

Figure 1
Purification of RVV-V. Crude venom (20 µg) and purified RVV-V (4 µg) were loaded on 4–12% SDS–PAGE in the presence or absence of 10 m*M* dithiothreitol. Proteins were stained with Coomassie Brilliant Blue. Lane 1, molecular-weight markers (kDa). Lanes 2 and 5, crude venom from *D. russelli siamensis*. Lanes 3 and 6, RVV-V purified by gel-filtration chromatography. Lanes 4 and 7, RVV-V purified by cation-exchange chromatography. Lanes 2–4 are under nonreducing conditions [DTT(−)] and lanes 5–7 are under reducing conditions [DTT(+)].

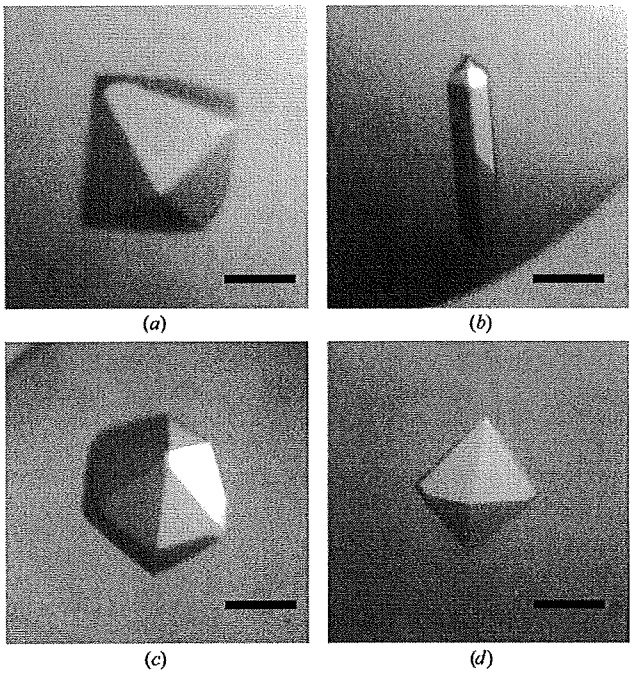

Figure 2
Crystals of RVV-V obtained under different conditions. (*a*) Form 1, (*b*) form 2, (*c*) form 3 (complexed with Pefabloc) and (*d*) form 4 (complexed with PPACK). The scale bar is 0.1 mm in length.

Table 1
Data-collection statistics for RVV-V crystals.

Values in parentheses are for the highest resolution shell.

	Form 1	Form 2	Form 3	Form 4
Inhibitor	None	None	Pefabloc	PPACK
X-ray source	SPring-8 BL41XU			
Space group	$P6_522$	$P6_522$	$P6_522$	$P6_522$
Unit-cell parameters				
a (Å)	78.9	80.1	78.9	77.2
b (Å)	78.9	80.1	78.9	77.2
c (Å)	157.3	160.4	160.6	168.4
$\alpha = \beta$ (°)	90	90	90	90
γ (°)	120	120	120	120
Resolution (Å)	50–1.9 (1.97–1.9)	50–1.9 (1.97–1.9)	30–2.85 (2.95–2.85)	30–2.55 (2.64–2.55)
No. of reflections	23547 (2301)	24182 (2389)	7400 (708)	10311 (993)
R_{merge}†	0.06 (0.255)	0.05 (0.282)	0.06 (0.319)	0.06 (0.267)
$I/\sigma(I)$	22.8 (8.64)	22.0 (7.13)	40.6 (12.3)	33.8 (15.8)
Completeness (%)	99.8 (100)	97.6 (99.5)	99.9 (100)	99.7 (100)
Redundancy	7	7.2	20.7	20.4
No. of molecules in ASU	1	1	1	1
Matthews value (Å^3 Da^{-1})	2.66	2.78	2.70	2.69
Solvent content (%)	53.9	55.8	54.6	54.2

† $R_{merge} = \sum_{hkl}\sum_i |I_i(hkl) - \langle I(hkl)\rangle| / \sum_{hkl}\sum_i I_i(hkl)$, where $I_i(hkl)$ is the ith intensity measurement of reflection hkl and $\langle I(hkl)\rangle$ is its average.

the RVV-V–Pefabloc and RVV-V–PPACK complexes were initially obtained in a similar manner as form 1 crystals using solution No. 38 of the PEG/Ion 2 kit at 293 K.

Because the crystals obtained from the initial screen were too small for X-ray analysis, we optimized the crystallization conditions to obtain larger single crystals by lowering the precipitant concentration and changing the droplet size and pH. Larger form 1 crystals were obtained by mixing 0.5 µl protein solution and 0.5 µl of a reservoir solution containing 50 m*M* citric acid, 50 m*M* bis-tris propane pH 5.0 and 16%(*w*/*v*) PEG 3350 (Fig. 2*a*). Larger form 2 crystals were obtained by mixing 0.3 µl protein solution and 0.3 µl of a reservoir solution containing 0.8%(*w*/*v*) tryptone, 0.04 *M* Na HEPES pH 7.0 and 9.6%(*w*/*v*) PEG 3350 (Fig. 2*b*). Diffraction-quality crystals of form 3 (RVV-V–Pefabloc complex) and form 4 (RVV-V–PPACK complex) were obtained by mixing 0.5 µl protein solution and 0.5 µl of a reservoir solution containing 0.8%(*w*/*v*) tryptone, 0.04 *M* Na HEPES pH 7.0 and 9.6%(*w*/*v*) PEG 3350 (Figs. 2*c* and 2*d*).

Crystals with dimensions of 200 × 200 × 200 µm (forms 1, 3 and 4) or 300 × 50 × 50 µm (form 2) were formed after 3–7 d at 293 K.

3.3. X-ray analysis

Prior to data collection, single crystals were cryoprotected using a reservoir solution supplemented with increasing glycerol concentrations (5, 10, 15 and 20%) in order to avoid osmotic shock-induced cracking. All diffraction data sets were acquired with a Rayonix MX225HE CCD detector using the oscillation method on beamline BL41XU, with an oscillation angle of 1.0°, a wavelength of 1.0 Å and a crystal-to-detector distance of 160 mm. The unit-cell parameters and statistics for the data sets are summarized in Table 1.

The asymmetric unit of each crystal was estimated to contain one RVV-V molecule, with corresponding crystal volume per protein weight ratios of 2.66, 2.78, 2.70 and 2.69 Å^3 Da^{-1} for crystal forms 1, 2, 3 and 4, respectively (Matthews, 1968). Solvent-content estimations based on a single copy of the molecule per asymmetric unit gave values of 53.9, 55.8, 54.6 and 54.2% for crystals forms 1, 2, 3 and 4, respectively. The unit-cell parameters of these four crystal forms were similar to, but distinct from, each other, suggesting structural changes that depended on the pH or on inhibitor binding. Clear molecular-replacement (MR) solutions for each crystal form were obtained in space group $P6_522$ using *MOLREP* from the *CCP*4 suite (Vagin & Teplyakov, 1997) with Ancrod (61% sequence identity), a snake-venom protein C activator from *Agkistrodon contortrix contortrix* (PDB code 2aiq; Murakami & Arni, 2005), as the structural model. Structural analyses of these crystals together with MR phasing are ongoing.

We thank Mariko Tomisako for her help in the purification and crystallization experiments and the staff of SPring-8 for assistance with data acquisition. This work was supported in part by grants-in-aid from the Ministry of Health, Labour and Welfare of Japan, grants-in-aid from the Ministry of Education, Culture, Sports, Science and Technology of Japan and by a grant from the Takeda Science Foundation.

References

Dahlback, B. (1986). *J. Biol. Chem.* **261**, 9495–9501.
Hjort, P. F. (1957). *Scand. J. Clin. Lab. Invest.* **9**, 1–183.
Jenny, R. J., Pittman, D. D., Toole, J. J., Kriz, R. W., Aldape, R. A., Hewick, R. M., Kaufman, R. J. & Mann, K. G. (1987). *Proc. Natl Acad. Sci. USA*, **84**, 4846–4850.
Kane, W. H. & Davie, E. W. (1986). *Proc. Natl Acad. Sci. USA*, **83**, 6800–6804.
Kane, W. H. & Davie, E. W. (1988). *Blood*, **71**, 539–555.
Kisiel, W. (1979). *J. Biol. Chem.* **254**, 12230–12234.
Laemmli, U. K. (1970). *Nature (London)*, **227**, 680–685.
Mann, K. G. & Kalafatis, M. (2003). *Blood*, **101**, 20–30.
Matthews, B. W. (1968). *J. Mol. Biol.* **33**, 491–497.
Murakami, M. T. & Arni, R. K. (2005). *J. Biol. Chem.* **280**, 39309–39315.
Nesheim, M. E., Taswell, J. B. & Mann, K. G. (1979). *J. Biol. Chem.* **254**, 10952–10962.
Nicolaes, G. A. & Dahlback, B. (2002). *Arterioscler. Thromb. Vasc. Biol.* **22**, 530–538.
Otwinowski, Z. & Minor, W. (1997). *Methods Enzymol.* **276**, 307–326.
Rosing, J., Tans, G., Govers-Riemslag, J. W., Zwaal, R. F. & Hemker, H. C. (1980). *J. Biol. Chem.* **255**, 274–283.
Schiffman, S., Theodor, I. & Rapaport, S. I. (1969). *Biochemistry*, **8**, 1397–1405.
Segers, K., Rosing, J. & Nicolaes, G. A. (2006). *Proteins*, **64**, 968–984.
Takeda, S., Igarashi, T. & Mori, H. (2007). *FEBS Lett.* **581**, 5859–5864.
Thorelli, E., Kaufman, R. J. & Dahlback, B. (1998). *Thromb. Haemost.* **80**, 92–98.
Tokunaga, F., Nagasawa, K., Tamura, S., Miyata, T., Iwanaga, S. & Kisiel, W. (1988). *J. Biol. Chem.* **263**, 17471–17481.
Vagin, A. & Teplyakov, A. (1997). *J. Appl. Cryst.* **30**, 1022–1025.